buildings

MDPI

Article

Risk Assessment of Long-Span Steel-Truss-Girder Cable-Stayed Bridge with Single Cable Plane and Single Pylon

Huijun Zheng [1,2,3,*], Yong Zeng [1,2,*], Hongmei Tan [1,2] and Qianping Zhang [1,4]

[1] State Key Laboratory of Mountain Bridge and Tunnel Engineering, Chongqing Jiaotong University, Chongqing 400074, China; hmtan@cqjtu.edu.cn (H.T.); zhangqianping24@outlook.com (Q.Z.)
[2] Mountain Bridge and Materials Engineering Research Center of Ministry of Education, Chongqing Jiaotong University, Chongqing 400074, China
[3] Department of Architectural Engineering, Hebei Petroleum University of Technology, Chengde 067000, China
[4] Guangxi Traffic Construction Engineering Testing Consulting Co., Ltd., Nanning 530001, China
* Correspondence: 227023@hebpu.edu.cn (H.Z.); yongzeng@cqjtu.edu.cn (Y.Z.); Tel.: +86-18731400235 (H.Z.)

Abstract

Long-span single-cable-plane rail-cum-road steel-truss-girder cable-stayed bridges are characterized by complex construction conditions, coupled loading effects, and uncertainties in construction parameters. Conventional risk assessment methods may be limited in quantitative accuracy and computational efficiency, particularly for pre-construction probabilistic prediction. Taking the Qiansimen Jialing River Bridge in Chongqing as the engineering background, this study integrates the analytic hierarchy process (AHP), grey relational analysis, finite element simulation, a radial basis function (RBF) neural network, and Monte Carlo simulation to establish an integrated probabilistic risk assessment framework for bridge construction. Numerical results show that the comprehensive displacement failure probability of the bridge at the maximum cantilever construction stage is 0.12%, indicating a low probability of displacement-related failure under the considered conditions. Cable elastic modulus and initial strain are the dominant parameters affecting cantilever alignment. A 6% deviation from their mean values increases the cantilever displacement by 5.93% and 4.89%, respectively, whereas cable density and Poisson's ratio have limited effects on structural deformation. The proposed multi-algorithm framework improves the computational efficiency of stochastic probabilistic simulation and provides a quantitative approach for parameter sensitivity analysis and pre-construction risk assessment of this bridge type. The results provide a reference for construction risk control, parameter regulation, and construction scheme optimization for similar urban cross-river rail-cum-road cable-stayed bridges.

Keywords: construction risk analysis; analytic hierarchy process; cable-stayed bridge; artificial neural network; Monte Carlo method; quantitative analysis

Check for updates

Academic Editor: Antonio Caggiano

Received: 2 April 2026
Revised: 27 September 2026
Accepted: 26 October 2026
Published: 2 November 2026

Copyright: © 2026 by the authors. Licensee MDPI, Basel, Switzerland. This article is an open access article distributed under the terms and conditions of the Creative Commons Attribution (CC BY) license.

1. Introduction

Long-span rail-cum-road cable-stayed bridges are widely used in urban river-crossing transportation systems because of their structural efficiency, spanning capability, and compatibility with urban landscapes. Compared with conventional single-purpose bridges, rail-cum-road composite cable-stayed bridges involve more complex construction systems, and their structural states vary throughout the construction process. Simultaneous exposure to loads associated with highway traffic and urban rail transit may introduce

additional construction uncertainties and safety risks. Bridge construction accidents involving structural collapse and component failure have caused casualties and economic losses. Reported cases include the main girder collapse of Zhouhe Bridge (1987), the compressive component failure of Zhaobaoshan Bridge (1998), the construction bracket collapse of Hangbu River Extra-large Bridge (2021), the hanging basket collapse of Tanjiang Extra-large Bridge (2024), the overall collapse of Jianzha Yellow River Extra-large Bridge in Qinghai (2025), and the collapse of the Agwani-Sultanganj extradosed cable-stayed bridge in India. These cases indicate that the construction of long-span rail-cum-road cable-stayed bridges can be affected by multiple, coupled, and stochastic risk factors. Therefore, systematic construction risk analysis and an appropriate risk assessment and control framework are required to support construction safety and risk-informed management [1,2].

Current studies on bridge construction risk assessment generally involve three categories of methods: probabilistic quantitative risk analysis [3], artificial intelligence-assisted reliability evaluation [4–8], and digital twin-based structural monitoring [9–11]. Although these approaches have established theoretical foundations and have been applied in engineering practice, limitations remain when they are used for the construction of long-span rail-cum-road cable-stayed bridges. Probabilistic risk assessment methods based on Monte Carlo simulation [12], Bayesian networks [6], and fault tree analysis [7] can represent parametric uncertainty, estimate structural failure probabilities, and identify failure paths. However, many studies focus on in-service bridges, whereas quantitative investigations covering the construction process of rail-cum-road cable-stayed bridges remain limited. In addition, some studies use standalone algorithms without direct integration with finite element-based structural simulation, which may limit their ability to represent construction-stage structural responses. Artificial intelligence-based reliability analyses commonly use models such as back-propagation (BP) neural networks and support vector machines (SVMs) [13] to approximate nonlinear relationships. Their performance, however, depends on the characteristics and representativeness of the training data, and complex coupled construction conditions may increase modelling difficulty. Digital twin technology combines sensor data acquisition and three-dimensional modeling for real-time status monitoring and warning. However, monitoring alone does not provide risk-factor weighting, construction scheme optimization, or probabilistic failure assessment. These limitations motivate the development of an integrated framework that combines complementary methods for pre-construction risk assessment and decision support.

To establish the methodological basis for the proposed framework, this study compares the functions and limitations of AHP, probabilistic models, surrogate models, and grey system theory. The comparison focuses on their roles in risk identification, uncertainty quantification, construction scheme evaluation, and computational analysis, as summarized in Table 1.

The comparison in Table 1 shows that individual risk assessment methods have different functional strengths and limitations. No single method considered here covers all five functions required in the proposed construction risk workflow: risk identification, weight calibration, construction scheme optimization, efficient computation, and probabilistic quantification. The analytic hierarchy process (AHP) [14–17] supports hierarchical decomposition of risk factors and indicator weighting, although the results can still be influenced by expert judgement. Conventional probabilistic models account for parameter uncertainty and can be used to estimate structural failure probabilities and corresponding risk levels. The radial basis function neural network (RBFNN) [18–21] can approximate nonlinear relationships and reduce the computational demand associated with repeated finite element analyses when an adequately validated surrogate model is available. Grey system theory (GST) [22–25] can support decision analysis under limited or uncertain information and is

therefore used here for construction alternative evaluation. These complementary functions provide the basis for integrating the methods into a unified workflow. Existing hybrid frameworks, however, may not simultaneously include construction scheme optimization, surrogate-based probabilistic analysis, treatment of coupled loading characteristics, and pre-construction assessment. The present study therefore integrates these functions for the specific construction conditions considered.

Table 1. Comparative analysis of advantages, disadvantages and research gaps of conventional risk assessment methods for cable-stayed bridge construction.

Research Methods	Core Advantages	Inherent Limitations	Engineering Applicability
Analytic hierarchy process (AHP)	This method allows for multi-dimensional and multi-layered decomposition of risk factors, achieves structured weighting of evaluation indicators, and can reduce subjective human biases. With systematic capability in risk identification, it is applicable to complex bridge construction conditions characterized by multi-factor coupling.	This approach merely supports semi-quantitative analysis and is unable to compute structural failure probabilities. It lacks the functions of dynamic risk evolution and probabilistic quantification, rendering precise risk classification unattainable.	This approach facilitates risk collation and indicator weight determination for complex construction scenarios, yet it is incapable of standalone quantitative risk assessment.
Traditional probabilistic models (Monte Carlo simulation; Bayesian networks)	This method fully accounts for parametric stochastic uncertainties, allows quantification of risk probabilities and recognition of structural failure paths, facilitates dynamic updating of risk levels, and achieves quantitative capability.	This method suffers from weak autonomous risk identification capability and limited applicability to practical engineering scenarios. When coupled with finite element simulations for co-calculation, it imposes substantial computational burdens and exhibits poor computational efficiency, rendering it unsuitable for large-scale iterative computations.	This approach is applicable to quantitative risk analysis yet cannot achieve systematic risk identification when used alone.
Back-propagation neural network, Kriging [6,8], and Gaussian process regression (GPR) [7,11]	This model has a simple structure and low requirements for engineering application. It enables fundamental nonlinear data fitting and achieves stable fitting performance under low-dimensional simple working scenarios.	This algorithm is characterized by slow convergence and easy trapping in local optima. It possesses poor generalization capability for bridge construction scenarios with high dimensionality and strong nonlinearity, accompanied by degraded computational stability and unsatisfactory calculation accuracy in large-scale sample computation.	This approach is merely adapted for static risk assessment of conventional standard bridges, which cannot fulfil the quantitative and dynamic solving requirements of long-span cable-stayed bridges.
Radial basis function neural network (RBFNN)	It possesses fast convergence speed, high fitting accuracy for high-dimensional nonlinear characteristics and generalization ability. It can efficiently couple finite element simulation and probabilistic simulation, thereby improving computational efficiency.	This model is not equipped with a built-in error assessment function, and its fitting precision is strongly contingent on high-quality and standardized training samples.	This model can accommodate intricate construction scenarios of long-span cable-stayed bridges and act as an efficient intelligent surrogate model to alleviate computational bottlenecks.
Grey system theory	It adapts to complex construction systems with poor information and high uncertainty, possesses strong robustness against data disturbance, and facilitates intelligent optimization and comparative analysis of multiple construction schemes.	This method merely enables qualitative analysis and construction scheme optimization, yet it lacks the capability to quantify risk probabilities and identify structural failure modes.	It bridges risk assessment and construction decision-making, thus remedying the disconnection between theoretical evaluation and practical engineering implementation.

Bridge risk assessment has increasingly incorporated probabilistic analysis, surrogate modelling, and data-assisted monitoring. However, quantitative studies that integrate construction scheme evaluation with probabilistic assessment for single-pylon, single-cable-plane rail-cum-road cable-stayed bridges remain limited. This study therefore uses the Qiansimen Jialing River Bridge in Chongqing as an engineering case. The bridge has a span arrangement of 80 m + 240 m + 312 m + 88 m and a total length of 720 m (Figures 1 and 2). Its single-cable-plane steel-truss-girder system, constrained urban construction site, and combined highway–rail configuration provide a representative case for examining construction-stage risk under coupled structural and parameter uncertainties.

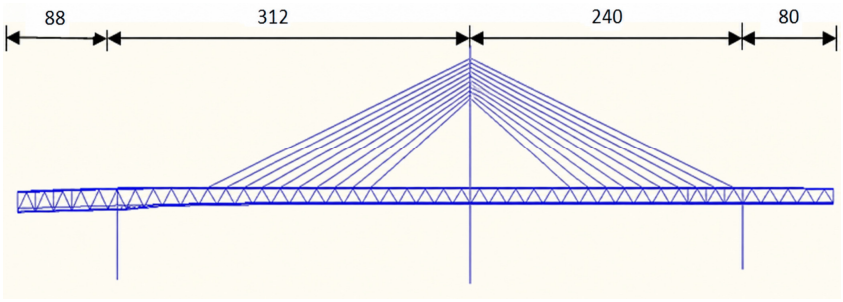


Figure 1. The overall layout (unit: m).



Figure 2. In situ.

The methodological contributions of this study are fourfold. First, AHP, grey relational analysis, finite element simulation, an RBF neural-network surrogate, and Monte Carlo simulation are integrated into a construction risk assessment workflow, addressing the limited scope of individual methods. Second, the RBF surrogate reduces the need for repeated finite element analyses and improves the efficiency of large-sample probabilistic calculations while maintaining the validated prediction accuracy reported in Section 4. Third, the framework quantifies risk-factor weights and parameter sensitivities for the Qiansimen Jialing River Bridge, providing case-specific evidence for construction-stage risk control. Fourth, the framework links construction scheme evaluation with probabilistic risk assessment and provides a methodological basis for subsequent validation using additional bridge projects and field-monitoring data.

2. Analysis of Construction Procedures

2.1. Finite Element (FE) Model

The finite element platform ANSYS is utilized to establish the numerical model of Qiansimen Jialing River Bridge under the maximum cantilever condition. Specifically,

the bridge deck plane is defined as the XY plane, where the longitudinal bridge direction corresponds to the X-axis, the transverse bridge direction corresponds to the Y-axis, and the vertical direction corresponds to the Z-axis. The developed model consists of 16,571 elements in total. The spatial truss element LINK10 is adopted to simulate stay cables, the BEAM4 element is applied for the bridge pylon, and the BEAM188 element is selected for the steel truss main girder. The numerical model for the maximum cantilever construction stage is displayed in Figure 3.

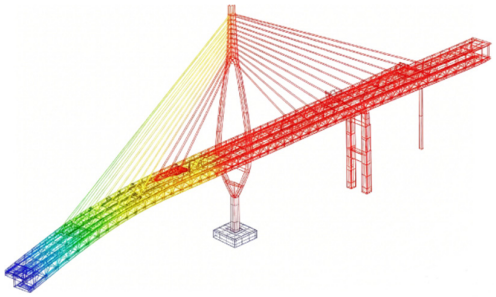


Figure 3. FE numerical model for maximum cantilever stage.

The different colors represent different displacement ranges in the finite element model.Material parameters corresponding to the actual construction stage of the bridge structure are adopted in the numerical model, as summarized in Table 2.

Table 2. Material property parameters for finite element modelling.

Component Description	Poisson's Ratio	Elastic Modulus/GPa	Mass Density/kg/m^{-3}
C50 Concrete Pylon	0.2	34.5	2.549
Stay Cables	0.3	195	8.005
Q370 Structural Steel	0.3	206	7.850
Rigid Links	0.3	206,000	0.000
Temporary Construction Falsework	0.3	206	7.850
Bridge Bearings	0.3	100,000	0.000
Longitudinal Bracing for Stay-Cable Cross Beams	0.3	54	7.850

In accordance with the staged construction sequence, the displacement occurring at the tip of the maximum cantilever under self-weight loads is adopted as the verification criterion for the bridge model. The critical cross-section for calculation is illustrated in Figure 4.

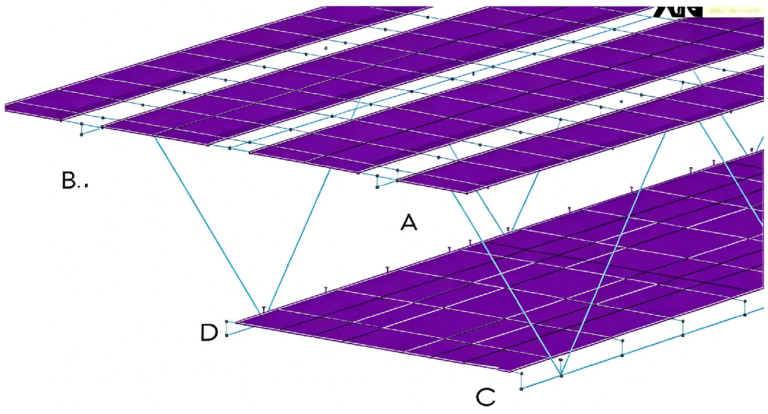


Figure 4. Critical cross-section for numerical calculation. A, B, C, and D denote the cross-sections corresponding to the four corner points at the leftmost end of the double-deck bridge.

2.2. Numerical Results

Using the foregoing material parameters, numerical simulations are carried out on the ANSYS finite element model to derive the displacement values of different critical cross-sections at the maximum cantilever tip of the cable-stayed bridge, as summarized in Table 3.

Table 3. Maximum displacement values of critical cross-sections.

Cross-section	A-A	B-B	C-C	D-D
Displacement/m	0.27	0.26	0.25	0.25

Finite element analysis can yield the structural responses of the bridge under designated load cases and parameter configurations. Nevertheless, the parameters of all construction materials adopted for the bridge are not deterministic constants but random variables. To quantify the risks arising during structural construction, a sufficient number of material parameter samples must satisfy the criteria of statistical regularity. In this context, carrying out extensive finite element simulations using commercial software becomes computationally impractical.

3. Risk Analysis Framework

This study integrates five complementary methods: analytic hierarchy process (AHP), grey relational analysis, finite element modelling, an RBF neural network [26–29], and Monte Carlo simulation [30–35]. AHP is used to determine risk-factor weights, grey relational analysis to compare construction alternatives, finite element modelling to generate structural response samples, the RBF network to approximate the input–response relationship, and Monte Carlo simulation to estimate failure probabilities. The resulting workflow supports construction-stage probabilistic risk assessment while reducing repeated finite element calculations.

Analytic hierarchy process (AHP) : AHP decomposes the construction risk problem into a hierarchy and assigns weights to risk indicators using expert pairwise comparisons. In this study, it is used to identify higher-priority indicators and provide weights for the subsequent scheme evaluation.

Grey relational analysis (GRA) [36,37]: GRA is used to compare cable-plane alternatives when the available information is limited and the indicators have different dimensions. Combined with the AHP-derived weights, it provides a quantitative basis for ranking the investigated construction schemes and identifying indicators for subsequent numerical analysis.

Radial basis function (RBF) neural network [38]: Repeated finite element analyses for large numbers of random parameter combinations are computationally demanding. The RBF neural network is therefore trained using finite element samples to approximate the nonlinear mapping between selected material parameters and structural displacement responses. After validation, it is used as a surrogate model in the Monte Carlo simulations. The adopted RBF structure is shown in Figure 5.

Monte Carlo theory [39]: Critical parameters, namely, elastic modulus, Poisson's ratio and initial cable strain of materials, obey stochastic probability distributions. By conducting sufficient random sampling, this theory applies the neural network surrogate model to implement massive working-condition simulations, replacing repetitive finite element calculations. The structural failure probability is obtained through probability statistics, which establishes a complete closed-loop workflow from qualitative weighting and scheme comparison to quantitative risk probability assessment.

The risk analysis framework is presented in Figure 6.

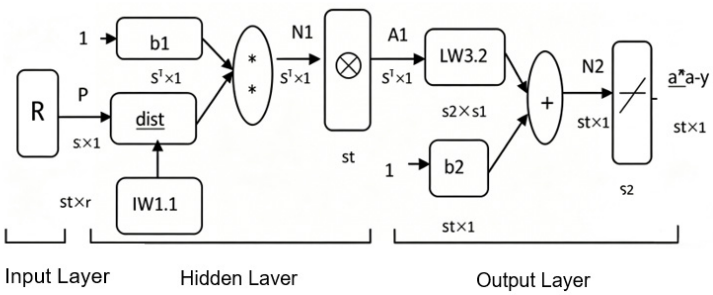


Figure 5. RBF neural network. The asterisks (*) denote element-wise multiplication of the distance vector by the hidden-layer bias vector to obtain the net input to the hidden layer.

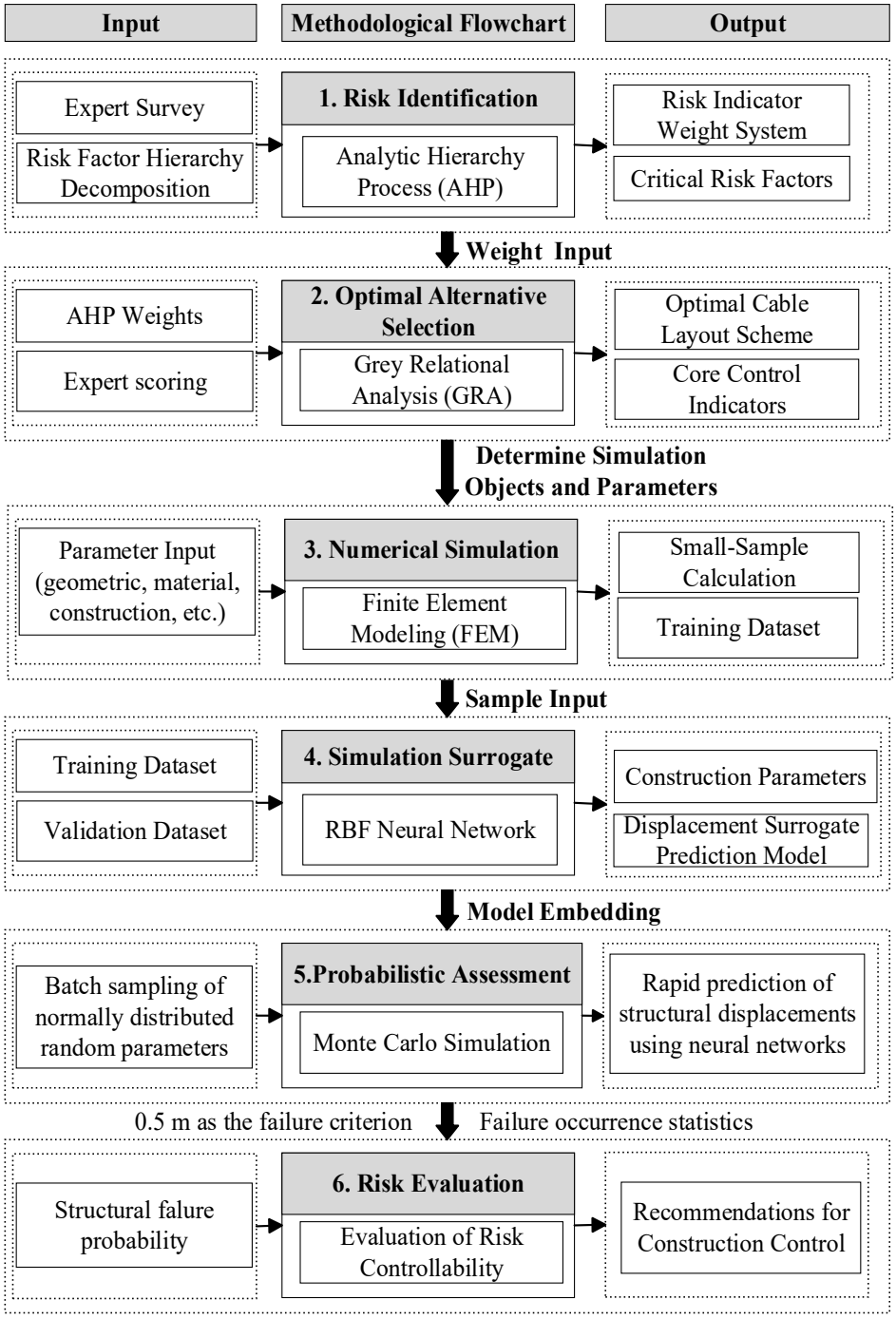


Figure 6. Flowchart for construction risk assessment.

3.1. Application of the Analytic Hierarchy Process in Construction Risk Assessment

Taking the overall construction risk of Qiansimen Bridge as the target layer, eight primary risk indicators are screened as the basic risk factors, including concrete performance, construction deviation, force majeure, integral main girder, temporary facilities, single girder member, stay-cable force and cable components. The corresponding analytic hierarchy structure diagram is presented in Figure 7.

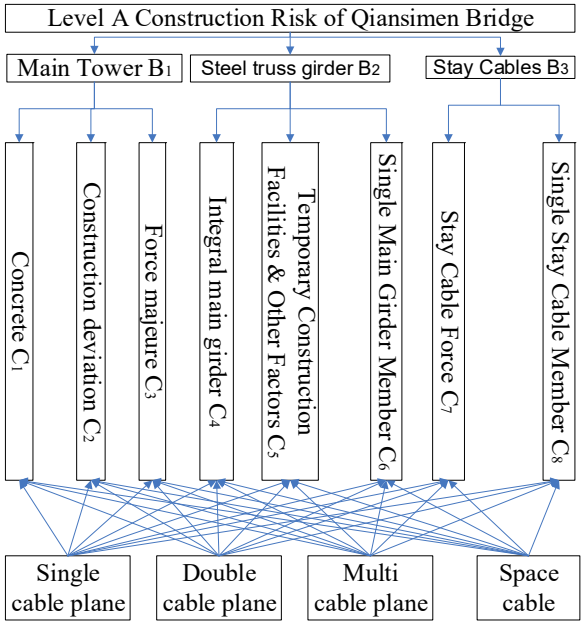


Figure 7. Risk hierarchy analysis diagram.

A total of 10 industry experts were recruited in this research, covering three groups of professionals: 3 project designers with more than 15 years of experience related to this project, 4 chief project engineers with over 12 years of on-site management experience on steel-truss-girder cable-stayed bridges, and 3 senior university researchers who have specialized in bridge risk research for more than 10 years. Such a multidisciplinary expert panel can effectively eliminate biases caused by a single research perspective. Questionnaire surveys and expert scoring were carried out. In accordance with the scoring criterion for pairwise importance comparison, the 1–9 scale of the analytic hierarchy process (AHP) (Table 4) was applied to establish judgement matrices.

To evaluate the consistency of the judgement matrix, consistency verification is carried out as follows:

$$\lambda_{\max} = \sum_{i=1}^{n} \frac{A \cdot W_{Ai}}{n \cdot W_{Ai}},\ CI = \frac{\lambda_{\max} - n}{n-1},\ CR = \frac{CI}{RI} \tag{1}$$

where

W_{Ai}: the i-th component of the weight vector of Layer A;
$\lambda_{\max}$: the maximum eigenvalue of the judgement matrix;
A: the judgement matrix;
n: the order of the judgement matrix;
CR: the consistency ratio; the consistency verification is deemed acceptable if $CR < 0.1$; otherwise, the judgement matrix needs to be inspected and revised;
RI: the random consistency index, with values presented in Table 5;
CI: the consistency index.

Table 4. Proportional scales for judgement matrices and their definitions.

Definitions	Scale Value
Element i and element j are of equal importance	1
Element i is slightly more important than element j	3
Element i is noticeably more important than element j	5
Element i is strongly superior in importance to element j	7
Element i is extremely more important than element j	9
The comparison result between element i and element j falls in the intermediate level of the above grades	2, 4, 6, 8
Let a_{ij} represent the judgement scale value when factor i is compared with factor j; accordingly, the judgement scale value for comparing factor j against factor i is $a_{ij} = 1/a_{ji}$, $a_{ii} = 1$	Reciprocals of the above scale values

Table 5. Random consistency RI value table.

Order n	1	2	3	4	5	6	7
RI	0	0	0.52	0.89	1.12	1.26	1.36

The calculated random consistency indices for each hierarchy are 0.0037, 0.0037 and 0, all below the standard threshold of 0.1, which verifies the consistency of the judgement matrix. Discrepancies in professional expertise, scoring tendencies and engineering practical backgrounds introduce subjective biases into expert scoring. In this research, artificial errors are alleviated by standardizing evaluation criteria in advance and eliminating outliers through consistency screening.

As revealed by the weighting results summarized in Table 6, the main girder obtains the highest weight of 0.4203, with cable force ranking second at 0.1723. From an engineering perspective, the bridge features a 720 m main span and a single-cable-plane steel truss girder constructed via large cantilever erection, which results in insufficient structural torsional stiffness. The stiffness and geometric alignment of the main girder serve as decisive factors governing stability throughout cantilever construction. The bridge adopts a double-deck layout to accommodate both rail transit and motor vehicle traffic. Any girder deformation not only jeopardizes structural safety during construction but also impairs the long-term service performance of the rail tracks. Various assembly tolerances and fluctuations in cable force will eventually trigger changes in the internal forces and displacements of the main girder. Accordingly, the main girder is recognized as the paramount control target for construction risk management.

Table 6. Comprehensive hierarchical weights.

Risk Index	Weight/W_A	Risk Index	Weight/W_A
concrete	0.0280	temporary construction facilities and other factors	0.1489
construction deviation	0.0791	single main-girder member	0.0791
force majeure	0.0149	stay-cable forces	0.1723
integral main girder	0.4203	single stay-cable member	0.0574

3.2. Grey Relational System Theory

Grey system theory is developed for uncertain systems with small sample sizes and limited available information, in which only partial information is accessible while the rest

is unknown. By comparing the geometric correlations of statistical sequences, this theory can quantify the relational degree between multiple influencing factors in a system.

The evaluation system for structural schemes of the Qiansimen Bridge consists of abundant multi-level indicators affected by diverse uncertain influencing factors. These factors are mutually correlated, interact with one another, and even conflict with each other. Consequently, the selection of cable-plane structural schemes bears typical grey system characteristics. On this basis, the cable-plane alternatives of the cable-stayed bridge can be evaluated by adopting the model and calculation procedures of the Grey Analytic Hierarchy Process (GAHP).

1. Fundamental steps of the grey analytic hierarchy process (GAHP)

Assume that the evaluation framework constitutes a multi-level system with evaluation indicators. Given there are alternatives in the system, the sequence formed by the indicators of the i-th alternative is defined as: $y_i = \{y_i(1), y_i(2), \ldots, y_i(m)\}(i = 1, 2, \ldots n)$.

(1) Determine the optimal indicator set

$y_0 = \{y_0(1), y_0(2), \ldots, y_0(m)\}$, where each element corresponds to the optimal value of the respective indicator across all alternatives.

(2) Normalization of indicator values

Owing to dimensional disparities between different indicators, mathematical operations cannot be directly conducted on raw data. Accordingly, normalization of the original indicator values is essential.

$$x_i(j) = \frac{y_i(j) - \min\limits_i y_i(j)}{\max\limits_i y_i(j) - \min\limits_i y_i(j)},\ i = 1, 2 \ldots n; j = 1, 2 \ldots m \tag{2}$$

In the formula, $\min\limits_i y_i(j)$ and $\max\limits_i y_i(j)$ respectively stand for the minimum and maximum values of the j-th indicator among all n alternatives.

(3) Calculate the grey relational coefficients

$$\zeta_i(j) = \frac{\min\limits_i \min\limits_j |x_0(j) - x_i(j)| + \rho \max\limits_i \max\limits_j |x_0(j) - x_i(j)|}{|x_0(j) - x_i(j)| + \rho \max\limits_i \max\limits_j |x_0(j) - x_i(j)|},\ i = 1, 2 \ldots n; j = 1, 2 \ldots m \tag{3}$$

In the formula, $\zeta_i(j)$ denotes the relative difference in the j-th indicator between the comparison sequence x_i and the reference sequence x_0.

The grey relational coefficient matrix can be further derived as shown below:

$$E = \begin{bmatrix} \zeta_1(1) & \zeta_2(1) & \ldots & \zeta_n(1) \\ \zeta_1(2) & \zeta_2(2) & \ldots & \zeta_n(2) \\ \ldots & \ldots & \ldots & \ldots \\ \zeta_1(m) & \zeta_2(m) & \ldots & \zeta_n(m) \end{bmatrix}$$

(4) Determination of indicator importance weights

$$W = \begin{bmatrix} w_1 & w_2 & \ldots & w_m \end{bmatrix}^T,\ j = 1, 2 \ldots m,\ \text{Where} \sum_{j=1}^{m} W_m = 1$$

(5) Calculation of grey relational degrees and determination of evaluation results for the optimal alternative

The comprehensive evaluation result is calculated as follows: $R = E \times W$

$$r_i = \sum_{j=1}^{m} \zeta_i(j) \times W(j),\ i = 1, 2 \ldots n; j = 1, 2 \ldots m \tag{4}$$

2. Application of the grey analytic hierarchy process (GAHP)

Experts were invited to assign scores of 10, 9, 8, 7, 6, 5, 4, 3, 2, and 1 to the four construction schemes according to the importance of each risk factor, as summarized in Table 7. A higher score means the scheme is closer to the optimal solution, which implies that the corresponding risk factor exerts a slighter influence on the construction scheme.

Table 7. Influence of structural parameters on diverse structural forms.

Structural Forms	Single-Cable-Plane Design	Double-Cable-Plane Design	Multi-Cable-Plane Design	Space Cable Design
concrete	7	3	6	5
construction deviation	10	7	10	7
force majeure	8	7	8	6
integral main girder	6	3	7	5
temporary construction facilities and other factors	8	5	3	4
single main girder member	7	5	4	6
Stay-cable force	9	8	7	4
single stay cable member	8	5	7	6

(1) Based on grey relational analysis, optimal indicators are chosen to form the reference sequence {7, 10, 8, 7, 8, 7, 9, 8}

(2) The original and optimal indicator sets are subjected to normalization.

The concrete indicator is subjected to normalization in accordance with Equation (2), and the derived result is:

$$X_S(C_1) = \frac{7-3}{7-3} = 1.00$$

$$X_D(C_1) = \frac{3-3}{7-3} = 0.00$$

$$X_M(C_1) = \frac{6-3}{7-3} = 0.75$$

$$X_{SP}(C_1) = \frac{5-3}{7-3} = 0.50$$

Similarly, the rest of the indicator data can be normalized using Equation (2) to obtain the values of comparison sequences and reference sequences (i.e., normalized indicator data), as shown in Figure 8.

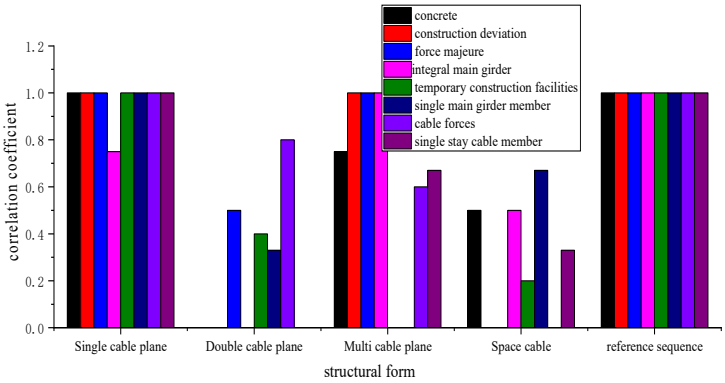


Figure 8. Evaluation of main tower influence on diverse structural forms.

As reflected by the standardized indicator scores of all schemes, the single-cable-plane design yields values close to the optimum for high-weight indicators, namely, overall girder performance, cable force, and construction deviation. Given the constrained construction space of urban project sites, double-cable-plane and spatial cable-stayed systems feature

intricate cable layouts and substantial expenditures on temporary works. Such characteristics lead to elevated risks for the associated indicators, which align with the typical construction patterns of real-world bridges.

(3) Calculation of grey relational coefficients

Equation (3) is utilized to compute the values of comparison sequences and the reference sequence acquired from the foregoing grey relational analysis, from which the grey relational coefficients of the indicator system for cable-stayed structural scheme selection are derived.

$$\min_i \min_j |x_0(j) - x_i(j)| = 0$$

$$\max_i \max_j |x_0(j) - x_i(j)| = 1$$

Let ρ = 0.5, whereby:

$$\zeta_S(c_1) = \frac{0 + 0.5 \times 1}{|1 - 1| + 0.5 \times 1} = 1.00$$

$$\zeta_D(c_1) = \frac{0 + 0.5 \times 1}{|1 - 0| + 0.5 \times 1} = 0.33$$

$$\zeta_M(c_1) = \frac{0 + 0.5 \times 1}{|1 - 0.75| + 0.5 \times 1} = 0.67$$

$$\zeta_{SP}(c_1) = \frac{0 + 0.5 \times 1}{|1 - 0.5| + 0.5 \times 1} = 0.50$$

Similarly, the grey relational coefficients of the remaining indicator data are calculated with the foregoing formula, and the calculation results are illustrated in Figure 9.

The grey relational coefficients of individual indicators demonstrate that the single-cable-plane design attains the maximum relational values for overall girder performance and cable force. Single-cable-plane layouts possess uncomplicated force transmission paths and enable straightforward regulation of cable tensioning. This observation aligns well with the findings of prior engineering studies.

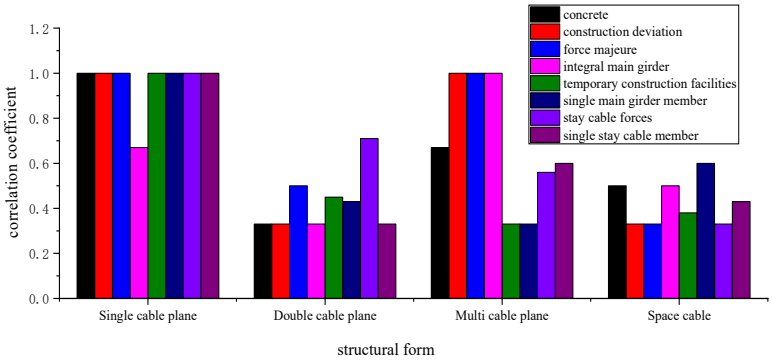


Figure 9. Grey relational coefficients between individual indicators and the optimal indicator.

(4) Determination of importance weights for evaluation indicators

The weight vector distribution values of eight evaluation indicators are obtained via the analytic hierarchy process (AHP), and the corresponding results are illustrated in Figure 10.

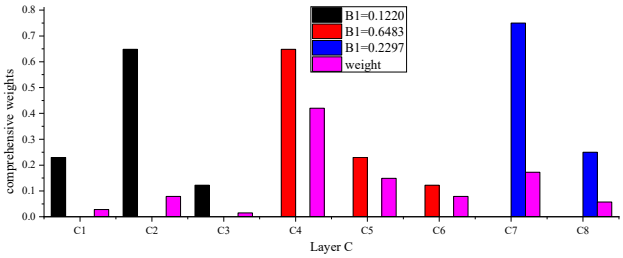


Figure 10. Comprehensive weights from analytic hierarchy process.

(5) Calculate the correlation degrees and determine the evaluation results of the optimal scheme.

The grey correlation degree of the i-th scheme is expressed as: $R_i = \sum_{j=1}^{m} W(j) \times \zeta_i(j), (i = 1, 2, \ldots n; j = 1, 2 \ldots m)$.

Based on this formula, the correlation values R_S, R_D, R_M and R_{SP} are calculated and plotted in Figure 11.

$$R_S = 1 \times 0.028 + 0.0791 + 0.0149 + 0.67 \times 0.4203 + 0.1489 + 0.0791 + 0.1723 + 0.0574 = 0.8613$$

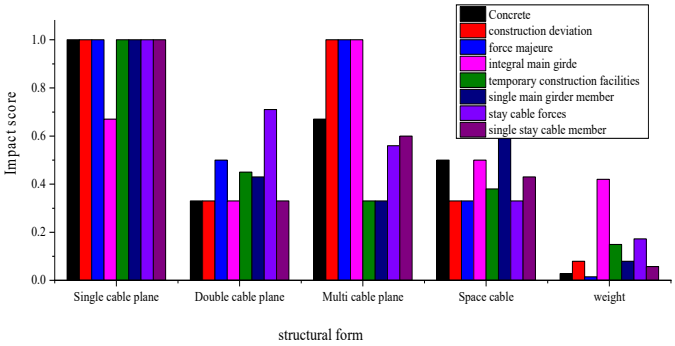


Figure 11. Grey relational coefficients of each secondary indicator and their respective weights in the comprehensive evaluation system.

Similarly, the grey relational coefficients of double-cable-net, multi-cable-net and spatial cable–membrane structural configurations can be quantified using the aforementioned identical method. The grey relational degrees for each structural form are obtained as:

$$R_D = 0.4238,\ R_M = 0.7392,\ R_{SP} = 0.4408$$

The AHP-weighted grey relational analysis ranks the investigated cable-plane alternatives according to their comprehensive relational degrees. Under the evaluation criteria and engineering conditions considered, the single-cable-plane scheme obtains the highest comprehensive grey relational degree, consistent with the configuration adopted for the Qiansimen Jialing River Bridge. The main girder has the largest indicator weight (0.4203), followed by stay-cable force and temporary works. These results indicate that girder performance, cable-force control, and temporary construction measures are important considerations in scheme evaluation. This analysis provides quantitative support for comparing the investigated alternatives; however, the result is specific to the selected indicators, expert-derived weights, and project conditions and should not be interpreted as general superiority of the single-cable-plane scheme for other bridges.

4. Analysis of Structural Failure Risk Probability

4.1. Generation of Training Samples for Neural Networks

The maximum cantilever construction stage is the most unfavourable governing working condition for the entire bridge. In accordance with the current code Design Specifications for Highway Cable-Stayed Bridges (JTG/T 3365-01—2020) [40], and considering the structural and construction characteristics of the Qiansimen Jialing River Bridge—including its low torsional stiffness of the single cable plane, dual rail-road deck operation, and cantilever assembly construction—the allowable vertical displacement limit at the cantilever tip is determined as 0.5 m based on finite element trial calculations and comprehensive engineering experience [41].

Four parameters following normal distributions—cable mass density, elastic modulus, Poisson's ratio and initial strain—are chosen to form the fundamental input vector R (Table 8). Vertical displacements measured at four critical sections (A, B, C and D) serve as the output variables of the neural network [42].

Table 8. Parameters of random distribution.

Variable	Average	Variation
Mass density	8.005	0.05
Elastic modulus	195	0.06
Poisson's ratio	0.3	0.05
Initial strain	0.003	0.06

4.2. Development and Validation of the RBF Neural Network Surrogate Model

To reduce the computational cost associated with repeated finite element analyses in the subsequent Monte Carlo simulation, an RBF neural network was constructed as a surrogate model to approximate the nonlinear relationship between uncertain cable parameters and structural displacement responses. Four uncertain parameters, namely, mass density, elastic modulus, Poisson's ratio, and initial strain, were taken as the input variables, while the vertical displacements at sections A-A, B-B, C-C, and D-D were used as the output responses. The corresponding finite element responses were obtained through batch calculations in ANSYS 2021 R2 (ANSYS Inc., Canonsburg, PA, USA).

Before surrogate-model development, the generated dataset was examined for data integrity and duplicate input–output combinations. After removing duplicated cases, 150 independent input–output samples were retained. Because the four input parameters have different physical dimensions and numerical scales, min–max normalization was applied to map the input variables to the interval $[0, 1]$. This preprocessing reduces the influence of differences in parameter magnitude on network construction and numerical prediction. The training samples for the neural network are shown in Figure 12.

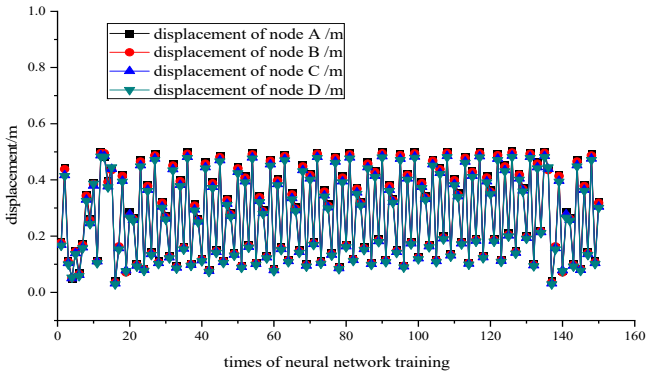


Figure 12. Neural network training samples.

4.2.1. Sample-Size Sensitivity Analysis

To quantitatively examine whether the available number of finite element samples was adequate for surrogate modelling, an additional sample-size sensitivity analysis was performed. A fixed set of 15 independent samples was reserved as the test set, while progressively enlarged training subsets containing 20, 40, 60, 80, 100, and 135 samples were selected from the remaining independent samples. The same test set and RBF model parameters were maintained for all sample-size conditions to ensure direct comparability. For training sizes smaller than 135, random subset selection was repeated to reduce the influence of individual sample selection.

The prediction performance was evaluated using the mean absolute error (MAE), root mean square error (RMSE), and coefficient of determination (R^2). The results are summarized in Table 9.

Table 9. Effect of training sample size on RBF surrogate-model performance.

Training Samples	MAE (m)	RMSE (m)	R^2
20	0.0824	0.1055	0.5295
40	0.0427	0.0623	0.8356
60	0.0336	0.0534	0.8765
80	0.0258	0.0467	0.9042
100	0.0211	0.0404	0.9295
135	0.0140	0.0243	0.9758

As the training sample size increased from 20 to 135, the MAE decreased from 0.0824 to 0.0140 m and the RMSE decreased from 0.1055 to 0.0243 m, while R^2 increased from 0.5295 to 0.9758. The results demonstrate a progressive improvement in predictive performance as additional finite element samples are incorporated. With 135 independent training samples, the model achieved an R^2 of approximately 0.976 on the fixed independent test set. Considering the prediction accuracy achieved and the computational cost associated with generating additional finite element samples, the available dataset was considered adequate for the present surrogate-model analysis. This conclusion applies specifically to the investigated parameter ranges and structural responses and does not imply that the adopted sample size is universally optimal.

4.2.2. RBF Model Construction and Accuracy Evaluation

The RBF surrogate model was implemented in MATLAB R2021a (MathWorks, Natick, MA, USA) using the newrbe function, while the structural responses used for model training and validation were obtained from the finite element model established in ANSYS 2021 R2 (ANSYS Inc., Canonsburg, PA, USA). The network consisted of four input neurons corresponding to the mass density, elastic modulus, Poisson's ratio, and initial strain of the stay cables, and four output neurons corresponding to the vertical displacements at sections A-A, B-B, C-C, and D-D. A single radial-basis hidden layer was adopted, with Gaussian radial basis functions in the hidden layer and a linear transfer function in the output layer. The number of hidden neurons was determined automatically by the newrbe network-construction procedure.

Prior to network construction, the input variables were normalized to the interval [0, 1] using min–max normalization in MATLAB. The normalization parameters determined from the training data were subsequently applied consistently to the independent test samples and Monte Carlo input samples. The spread parameter, which controls the width of the radial basis functions, was determined through preliminary validation trials. A spread value of 0.1 was adopted for the final model because it provided an appropriate balance between approximation accuracy and generalization performance for the present

dataset. The same spread value was maintained throughout the sample-size sensitivity analysis and subsequent probabilistic simulations.

The RBF network was constructed using the MATLAB (R2021a MathWorks, Natick, MA, USA)newrbe algorithm. Unlike gradient-based back-propagation neural networks, the adopted newrbe implementation does not employ conventional epoch-based iterative weight updating. Therefore, conventional epoch-based convergence criteria and stopping conditions were not applicable. Model adequacy was instead evaluated on the fixed independent test set using MAE, RMSE, and R^2. The final RBF model achieved an average MAE of 0.01402 m, an RMSE of 0.02434 m, and an average R^2 of 0.97578. These implementation settings were retained in the subsequent large-scale Monte Carlo simulations.

The final RBF model was trained using 135 independent samples and evaluated against the fixed set of 15 independent test samples. The predictive accuracy for the four investigated cross-sections is presented in Table 10.

Table 10. Prediction accuracy of the RBF surrogate model.

Cross-Section	MAE (m)	RMSE (m)	R^2
A–A	0.01486	0.02669	0.97206
B–B	0.01388	0.02368	0.97749
C–C	0.01367	0.02348	0.97671
D–D	0.01365	0.02335	0.97686
Average	0.01402	0.02434	0.97578

The coefficients of determination for the four investigated sections ranged from 0.9721 to 0.9775, with an average R^2 of 0.9758. The corresponding average MAE and RMSE were 0.0140 m and 0.0243 m, respectively. The relatively consistent accuracy across the four structural responses indicates that the RBF model captures the overall nonlinear relationship between the selected uncertain parameters and the cantilever displacement responses within the investigated parameter ranges.

4.2.3. Comparison with Alternative Surrogate Models

To further evaluate the predictive characteristics of the adopted surrogate model, quadratic polynomial regression and Kriging surrogate models were constructed using the same 135 training samples and 15 independent test samples. The same input and output variables were used for all three models to ensure a consistent basis for comparison. The quantitative results are presented in Table 11.

Table 11. Comparison of prediction accuracy among different surrogate models.

Model	MAE (m)	RMSE (m)	Average R^2
Polynomial regression	0.02082	0.02874	0.96613
Kriging	0.01862	0.02635	0.96986
RBF neural network	0.01402	0.02434	0.97578

As shown in Table 11, all three surrogate models were able to capture the overall nonlinear relationship between the uncertain input parameters and structural displacement responses, although differences in predictive accuracy were observed. The polynomial regression model yielded an MAE of 0.02082 m, an RMSE of 0.02874 m, and an average R^2 of 0.96613. The Kriging model showed improved predictive performance, reducing the MAE and RMSE to 0.01862 m and 0.02635 m, respectively, while increasing the average R^2 to 0.96986. Among the three models, the RBF neural network achieved the lowest MAE (0.01402 m) and RMSE (0.02434 m), together with the highest average R^2 (0.97578).

These results indicate that the RBF neural network provided the highest predictive accuracy among the three surrogate models under the same dataset and evaluation criteria. Compared with polynomial regression and Kriging, the RBF model reduced the MAE by approximately 32.7% and 24.7%, respectively, while maintaining an average R^2 close to 0.98. The results therefore support the use of the RBF neural network as the surrogate model for the subsequent large-scale Monte Carlo simulation. Nevertheless, the comparison is specific to the present dataset, parameter ranges, and model settings, and should not be interpreted as demonstrating the universal superiority of the RBF model over other surrogate techniques.

4.3. Risk Analysis Using a Neural Network Surrogate Model

4.3.1. Monte Carlo-Based Calculation of Structural Failure Probability

After full validation, the radial basis function (RBF) neural network surrogate model was adopted to replace the refined finite element model for batch stochastic calculations. Sampling analyses were conducted at three sample sizes of 500,000, 1,500,000, and 2,000,000. A vertical displacement of 0.5 m at the cantilever end was defined as the structural failure criterion, and the failure probability of each section was quantified according to the proportion of over-limit samples, with the statistical results summarized in Table 11. A convergence threshold was set whereby the relative error of failure probability between adjacent sample sizes was controlled within 1%. The variation in failure probability for all sections was less than 1% when the sample size increased from 1,500,000 to 2,000,000, verifying that the sample size of 2,000,000 is sufficiently reliable for numerical simulation. Based on the simulation results of 2,000,000 sampling cases, the normal approximation method was utilized to calculate the 95% confidence interval.

For each Monte Carlo sample, structural failure is treated as a Bernoulli event, with failure defined as a vertical displacement exceeding 0.5 m. Assuming independent and identically distributed samples, the failure probability is estimated as

$$\hat{P}_f = \frac{N_F}{N} \tag{5}$$

where N_f is the number of failure samples and N is the total number of samples.

Based on the normal approximation to the binomial proportion, the 95% confidence interval is calculated as

$$CI_{95\%} = \hat{P}_f \pm 1.96\sqrt{\frac{\hat{P}_f(1-\hat{P}_f)}{N}} \tag{6}$$

This approximation assumes independent Bernoulli trials with a constant failure probability. In this study, $N = 2.0 \times 10^6$ and $\hat{P}_f \approx 0.0012$, corresponding to approximately 2400 failure samples. Thus, both $N\hat{P}_f$ and $N\left(1-\hat{P}_f\right)$ are sufficiently large to support the normal approximation. Therefore, the above interval is appropriate for quantifying the sampling uncertainty of the estimated failure probability. The structural failure probability prediction results are presented in Table 12.

Table 12. Structural failure-probability prediction results.

Number of Computations	Section A-A	Section B-B	Section C-C	Section D-D
5×10^5	9.0200×10^{-4}	9.0400×10^{-4}	8.3400×10^{-4}	8.2800×10^{-4}
1.5×10^6	1.2800×10^{-3}	1.1500×10^{-3}	9.2600×10^{-4}	9.1700×10^{-4}
2.0×10^6	1.2100×10^{-3}	1.1700×10^{-3}	9.2900×10^{-4}	9.1400×10^{-4}

The failure probabilities of sections A-A to D-D ranged from 0.0914% to 0.121%. The relatively narrow confidence intervals indicate limited Monte Carlo sampling uncertainty at the adopted sample size. The comprehensive displacement failure probability at the maximum cantilever stage was approximately 0.12% under the specified parameter distributions and the 0.5 m displacement criterion. Figure 13 presents the corresponding displacement–probability-density curves. Most simulated displacement values are below the predefined threshold. For construction management, the results support attention to prefabrication and assembly accuracy, cantilever alignment, and cable-tension adjustment. These implications are specific to the analyzed construction stage and model assumptions.

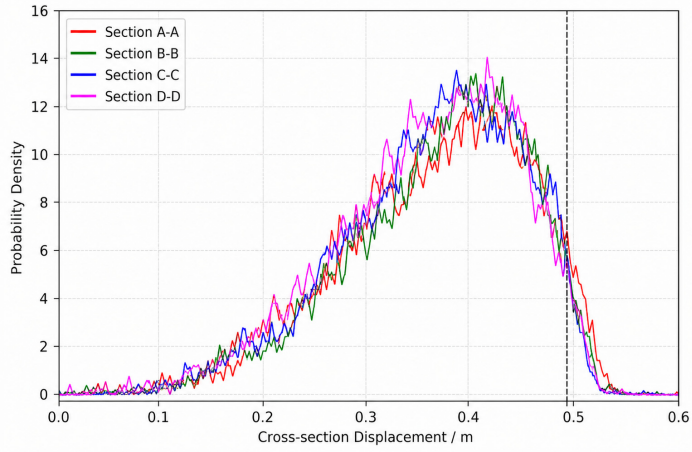


Figure 13. Probability-density curves of various sections.

4.3.2. Sensitivity Analysis of Key Parameters

To quantify the impacts of four categories of input parameters on cantilever displacement, sensitivity analysis is performed using the univariate perturbation method. With the values of other parameters kept constant, only a single parameter varies within the statistical range, and a well-trained RBF neural network model is adopted to determine the displacement fluctuation magnitude. The relative fluctuation amplitudes of the global maximum displacement are presented in Table 13.

Table 13. Relative fluctuation amplitude of global maximum displacement.

Ranking	Parameter Name	Maximum Fluctuation Amplitude of Global Displacement	Sensitivity Grade
1	Stay-Cable Elastic Modulus	5.93%	High Sensitivity
2	Stay-Cable Initial Strain	4.89%	High Sensitivity
3	Stay-Cable Mass Density	1.86%	Low Sensitivity
4	Stay-Cable Poisson's Ratio	0.94%	Low Sensitivity

The sensitivity analysis shows that a 6% deviation in cable elastic modulus and initial strain produces maximum displacement variations of 5.93% and 4.89%, respectively, whereas cable density and Poisson's ratio have smaller effects within the investigated ranges. These results suggest that elastic modulus and initial strain should receive greater attention in construction-stage parameter control, including material-property verification and cable-strain calibration during tensioning.

5. Main Conclusions

This study developed an integrated construction risk assessment framework for a long-span single-pylon, single-cable-plane steel-truss-girder cable-stayed bridge by combining the analytic hierarchy process (AHP), grey relational analysis, finite element simulation, an

RBF neural network, and Monte Carlo simulation. Based on the Qiansimen Jialing River Bridge, the main conclusions are summarized as follows:

(1) Risk-weight quantification

The AHP results identified the integral main girder and stay-cable force as the dominant construction risk indicators, with weights of 0.4203 and 0.1723, respectively. These results indicate that main-girder deformation and cable-force variation require particular attention during the maximum cantilever construction stage.

(2) Construction scheme evaluation

Grey relational analysis was used to evaluate the alternative cable-plane arrangements by incorporating the AHP-derived indicator weights. Among the investigated alternatives, the single-cable-plane scheme obtained the highest comprehensive grey relational degree, supporting its selection under the evaluation criteria and engineering conditions considered in this study.

(3) Surrogate-model performance

The RBF neural-network surrogate model reproduced the relationship between the selected random parameters and structural displacement responses with good accuracy. The R^2 values for the four investigated cross-sections ranged from 0.9721 to 0.9775, with an average R^2 of 0.9758; the corresponding average MAE and RMSE were 0.01402 m and 0.02434 m, respectively. Compared under the same dataset and evaluation criteria, polynomial regression and Kriging yielded average R^2 values of 0.9661 and 0.9699, respectively. These results support the use of the RBF model for the subsequent probabilistic simulations in this case.

(4) Failure-probability analysis

Monte Carlo simulation based on the validated RBF surrogate model showed stable failure-probability estimates as the sample size increased. Using 2,000,000 samples and a vertical displacement of 0.5 m as the failure criterion, the comprehensive displacement failure probability at the maximum cantilever stage was approximately 0.12%. This value applies to the parameter distributions, model assumptions, construction stage, and failure criterion adopted in this study 2.0×10^6.

(5) Parameter sensitivity

The single-factor perturbation analysis showed that the elastic modulus and initial strain of the stay cables were the most influential parameters affecting cantilever displacement. A 6% deviation from their mean values resulted in displacement variations of 5.93% and 4.89%, respectively, whereas cable density and Poisson's ratio produced comparatively small effects. Therefore, the elastic modulus and initial strain should receive greater attention in construction-stage parameter control.

(6) Engineering implications

The results provide a quantitative basis for identifying higher-priority construction risks, comparing cable-plane arrangements, and prioritizing parameter control for the case bridge. In construction management, particular attention may be given to main-girder deformation, cable-force adjustment, cable elastic modulus, and initial strain during the maximum cantilever stage. The surrogate-assisted probabilistic framework also reduces the number of repeated finite element analyses required for large-sample stochastic evaluation.

(7) Limitations

Several limitations should be acknowledged. First, the framework is evaluated using a single engineering case, and its transferability to other bridge types and construction

environments has not yet been established through multi-project validation. Second, field-monitoring data were not used to independently validate or update the probabilistic model. Third, the probabilistic analysis considers selected stay-cable parameters but does not explicitly include temperature effects, wind loads, assembly errors, and other construction disturbances. Finally, excessive vertical displacement is used as the principal failure criterion, and the analysis focuses on the maximum cantilever stage rather than the entire construction process.

(8) Future research

Future studies should validate the framework using additional bridge projects and incorporate field-monitoring data for model calibration and updating. Additional uncertainty sources, including environmental loads, construction deviations, and time-dependent parameter variations, should also be considered. Extending the assessment to multiple construction stages and multiple performance criteria would provide a broader basis for evaluating the applicability of the proposed approach.

Author Contributions: Conceptualization, H.Z.; methodology, H.Z.; software, Q.Z.; validation, H.T.; formal analysis, Q.Z. and H.Z.; investigation, H.Z.; writing—original draft preparation, H.T.; writing—review and editing, H.Z.; visualization, Y.Z.; supervision, H.Z.; funding acquisition, Y.Z. All authors have read and agreed to the published version of the manuscript.

Funding: This research was funded by the National Natural Science Foundation of China (No. 52478139), the State Key Laboratory of Bridge Safety and Resilience (2025SKLBSR-DW004), the Chongqing Science and Technology Commission (No. 2024NSCQ-MSX2566), and the Hubei Provincial Natural Science Foundation Innovation and Development Joint Fund Project (2026AFC1169).

Institutional Review Board Statement: Not applicable.

Informed Consent Statement: Not applicable.

Data Availability Statement: The datasets generated and analyzed during the current study, including the input parameter samples, finite element simulation results, and surrogate model datasets, are available from the corresponding author upon reasonable request.

Conflicts of Interest: Author Qianping Zhang was employed by the company Guangxi Traffic Construction Engineering Testing Consulting Co., Ltd. The remaining authors declare that the research was conducted in the absence of any commercial or financial relationships that could be construed as a potential conflict of interest.

References

1. Gong, C.; Cheng, J.; Shen, X. Research and application of analysis theory of long-span cable-stayed bridge construction risk. *City Bridg. Flood* **2012**, *2*, 117–118. (In Chinese)
2. Zhuang, M. Analysis of Minsheng Road Cable-Stayed Bridge Construction Control and Foundation Settlement. Master's Thesis, Dalian University of Technology, Dalian, China, 2009. Available online: https://kns.cnki.net/kcms2/article/abstract?v=x5ZT7qxuO_rGZT5lEjNDWHnRX_WyfAftOplGEzxWCTcnGDpgFdHnBWWO1l6yDBgGGUIPqmT9JlvFYSPThZj6fRy1DntNyF4Sp3JsbC3AUU-C30NPayRf7CNRMO5ZpclI7OtshK6mZRx3NNPhYrpcrlUeVUzmxO6Z3qTgH-zyPUTJ6gVNu2ZECA==&uniplatform=NZKPT&language=CHS (accessed on 25 March 2026). (In Chinese)
3. Hörteborn, A.; Sha, Y.; Ringsberg, J.W.; Mao, W.; Lundbäck, O. Risk Analysis Methodology for Ship-Bridge Allisions—A Combined Probability and Consequence Analysis. *Eng. Struct.* **2026**, *347*, 121731. [CrossRef]
4. Su, J.; Zhang, J.; Caprani, C.C.; Zhou, J. A practical framework for determining target reliability indices for the assessment of existing structures based on risk-informed decision-making. *Struct. Saf.* **2025**, *114*, 102583. [CrossRef]
5. Zhang, J.; Jing, Y.; Ma, J.; Luo, J.; Bao, H.; Chen, S. Machine learning enhanced bridge vulnerability quantification under rockfall hazards. *Eng. Geol.* **2025**, *352*, 108066. [CrossRef]
6. Luo, C.; Zhu, S.-P.; Keshtegar, B.; Macek, W.; Branco, R.; Meng, D. Active Kriging-based conjugate first-order reliability method for highly efficient structural reliability analysis. *Comput. Methods Appl. Mech. Eng.* **2024**, *423*, 116863. [CrossRef]

7. Xie, B.; Lin, L.; Liu, X.; Liu, K.; Wu, S. Engineering structural reliability analysis with multimodal uncertainties using adaptive polynomial chaos expansion. *Structures* **2026**, *87*, 111652. [CrossRef]
8. Kang, T.W.; Mo, Y. A comprehensive digital twin framework for building environment monitoring with emphasis on real-time data connectivity and predictability. *Dev. Built Environ.* **2024**, *17*, 100309. [CrossRef]
9. Yu, C.; Liu, Z.; Wang, H.; Shi, G.; Song, T. Intelligent Analysis of Construction Safety of Large Underground Space Based on Digital Twin. *Buildings* **2024**, *14*, 1551. [CrossRef]
10. Zhang, Y.; Zhao, Y.; Li, Z.; He, W.; Liu, Y. Research on the Digital Twin System for Rotation Construction Monitoring of Cable-Stayed Bridge Based on MBSE. *Buildings* **2025**, *15*, 1492. [CrossRef]
11. Zhang, H.; Yan, J.; Yang, J.; Meng, W.; Chen, S. Two-stage point cloud registration using multi-scale edge convolution for digital twin-based bridge construction progress monitoring. *Autom. Constr.* **2025**, *178*, 106415. [CrossRef]
12. Ji, Y.; Yao, B.; Xu, W. Research on Deflection Risk Assessment for Steel Box Girder Bridges Based on GA-BP Neural Network. *Buildings* **2024**, *14*, 3923. [CrossRef]
13. Wu, Y.; Wang, Y.; Liu, H.; Xie, L.; Jiao, L.; Lu, P. Risk assessment of bridge construction investigated using random forest algorithm. *Sci. Rep.* **2024**, *14*, 20964. [CrossRef]
14. Li, J.; Wang, J.; Zhao, X.; Wang, F.; Li, Y. Influence of Initial Conditions on Wind Characteristics at a Bridge Middle Span in a U-shaped Valley by CFD and AHP. *Appl. Sci.* **2022**, *12*, 4693. [CrossRef]
15. Liu, H.; Li, J.; Zhang, J.; Pang, D. Decision analysis of a reinforcement scheme for in-service prestressed concrete box girder bridges based on AHP and evaluation of the reinforcement effect. *Buildings* **2022**, *12*, 1771. [CrossRef]
16. Feng, S.; Lei, H.; Wan, Y.; Jin, H.; Han, J. Influencing factors and control measures of excavation on adjacent bridge foundation based on analytic hierarchy process and finite element method. *Front. Struct. Civ. Eng.* **2021**, *15*, 461–477. [CrossRef]
17. Su, H.; Guo, C.; Wang, Z.; Han, T.; Kamanda, D.B.; Su, F.; Shang, L. Research on safety condition assessment methodology for single tower steel box girder suspension bridges over the sea based on improved AHP-fuzzy comprehensive evaluation. *Sci. Rep.* **2024**, *14*, 12079. [CrossRef]
18. Fahmy, A.S.; El-Madawy, M.E.T.; Gobran, Y.A. Using artificial neural networks in the design of orthotropic bridge decks. *Alex. Eng. J.* **2016**, *55*, 3195–3203. [CrossRef]
19. Salehi, M.; Erduran, E. Identification of boundary conditions of railway bridges using artificial neural networks. *J. Civ. Struct. Health Monit.* **2022**, *12*, 1223–1246. [CrossRef]
20. Cao, Z.; Sun, B.; Zhou, G.; Mao, S.; Zhu, S.; Zhang, J.; Ke, C.; Zhao, Y.; Shao, J. Memristor-based neural networks: A bridge from device to artificial intelligence. *Nanoscale Horiz.* **2023**, *8*, 716–745. [CrossRef]
21. Xiao, H.; Huang, W.; Wang, J. Modeling Hurricane Wave Forces Acting on Coastal Bridges by Artificial Neural Networks. *J. Mar. Sci. Eng.* **2025**, *13*, 2080. [CrossRef]
22. Jiang, P.; Dong, Z.; Sun, H.; Song, Y.; Zou, Q. Grey system theory in supply chain. *Grey Syst. Theory Appl.* **2025**, *15*, 124–144. [CrossRef]
23. Yu, J.; Zhang, X.; Xiong, C. A methodology for evaluating micro-surfacing treatment on asphalt pavement based on grey system models and grey rational degree theory. *Constr. Build. Mater.* **2017**, *150*, 214–226. [CrossRef]
24. Qin, X.; Zha, X.; Wu, Z.; Zhang, L. Grey fuzzy comprehensive evaluation of bridge risk during periods of operation based on a combination weighting method. *Appl. Sci.* **2023**, *13*, 8964. [CrossRef]
25. Liu, S.; Tao, Y.; Xie, N.; Tao, L.; Hu, M. Advance in grey system theory and applications in science and engineering. *Grey Syst. Theory Appl.* **2022**, *12*, 804–823. [CrossRef]
26. Yuan, W.; Ding, T.; Hu, X.; Liu, J. Finite element analysis of the seismic performance of wind and rain bridge. *Sci. Rep.* **2025**, *15*, 26316. [CrossRef]
27. He, X.; Wang, Z.; Li, C.; Gao, C.; Liu, Y.; Li, C.; Liu, B. Experimental Test and Finite Element Analysis on a Concrete Box Girder of a Cable-Stayed Bridge with W-Shaped Prestressed Concrete Diagonal Braces. *Buildings* **2024**, *14*, 506. [CrossRef]
28. Qin, S.; Huang, J.; Li, S.; Zhou, Y.; Wahab, M.A. Novel two-stage adaptive weight coefficients for Finite Element Model Updating of a cable-stayed bridge via sensitivity analysis and Kriging model. *Mech. Syst. Signal Process.* **2025**, *231*, 11267. [CrossRef]
29. Xie, L.; Xu, Z.; Zheng, Z. Research on time-varying cable tension prediction of cable-stayed bridges based on short-term monitoring data and finite element results. *Eng. Res. Express* **2026**, *8*, 025109. [CrossRef]
30. Al Hawarneh, A.; Alam, M.S.; Ruparathna, R. Decision support framework for screening deficient bridges based on statistically-identified key indicators and Monte Carlo simulation. *Autom. Constr.* **2026**, *181*, 106624. [CrossRef]
31. Castellon, D.F.; Fenerci, A.; Øiseth, O.; Petersen, Ø.W. Investigations of the long-term extreme buffeting response of long-span bridges using importance sampling Monte Carlo simulations. *Eng. Struct.* **2022**, *273*, 114986. [CrossRef]
32. Castellon, D.F.; Fenerci, A.; Petersen, Ø.W.; Øiseth, O. Full long-term buffeting analysis of suspension bridges using Gaussian process surrogate modelling and importance sampling Monte Carlo simulations. *Reliab. Eng. Syst. Saf.* **2023**, *235*, 109211. [CrossRef]

33. Naderpour, H.; Kheyroddin, A.; Mortazavi, S. Risk assessment in bridge construction projects in Iran using Monte Carlo simulation technique. *Pract. Period. Struct. Des. Constr.* **2019**, *24*, 04019026. [CrossRef]
34. Sifre, S.P.; Lenner, R. Bridge assessment reduction factors based on Monte Carlo routine with copulas. *Eng. Struct.* **2019**, *198*, 109530. [CrossRef]
35. Cardoso, M.L.; Alencar, G.; Santos da Silva, J.G. Analysis methodology for dynamic structural behaviour modelling of highway bridges based on Monte Carlo simulations (MCS) considering vehicle-pavement-bridge interaction. *Int. J. Struct. Integr.* **2025**, *16*, 187–213. [CrossRef]
36. Shen, S.; Huang, Y.; Jones, A.S. Developing a three-level circular economy framework to measure circularity for meso-level assessment in pavement construction. *J. Clean. Prod.* **2026**, *542*, 147557. [CrossRef]
37. Wan, L.; Qiao, J.; Sun, Q.; Liu, J. Construction control of rigid frame-continuous girder bridge based on grey theory. *J. Eng. Appl. Sci.* **2024**, *71*, 171. [CrossRef]
38. Zhang, S.; Tan, Y.; Ge, H.; Zhang, Q. Safety–Function–Environment Evaluation System for Large-Span Cable-Supported Bridges: Theory and Case Studies. *Sustainability* **2024**, *16*, 1414. [CrossRef]
39. Yepes-Bellver, L.; Brun-Izquierdo, A.; Alcalá, J.; Yepes, V. Artificial neural network and Kriging surrogate model for embodied energy optimization of prestressed slab bridges. *Sustainability* **2024**, *16*, 8450. [CrossRef]
40. Liu, Z.; Fang, G.; Zhao, L.; Ge, Y.; Nikitas, N.; Zio, E. Extreme buffeting response of long-span bridges under probabilistic wind field: Environmental contours vs. brute-force Monte Carlo approaches. *Reliab. Eng. Syst. Saf.* **2026**, *270*, 112199. [CrossRef]
41. *JTG/T 3365-01—2020*; Ministry of Transport of the People's Republic of China. Specifications for Design of Highway Cable-Stayed Bridge. China Communications Press: Beijing, China, 2020.
42. Zheng, H. Construction Risk Analysis of a Large-Span Single-Plane Steel-Girder Cable-Stayed Bridge. Master's Thesis, Chongqing Jiaotong University, Chongqing, China, 2014. Available online: https://kns.cnki.net/kcms2/article/abstract?v=x5ZT7qxuO_rkbmX6DOZwGoXflxOiLWwFJCc72H4cI8h1xE3k0V8SUbqw8m0wkpOA-sOSUTGRGOf1EPjyPkxuBglFxzLOZKrCozhMGdcSgwAeqwXcL0NdVjErqAi5L_D6CIWRzjv7wW8ht6YUCHeO5VC5STcdFGhTfcZbHc8nGSXRJYQmUlQXmPv0Kb2Ibld8&uniplatform=NZKPT&language=CHS (accessed on 15 March 2026). (In Chinese)

Disclaimer/Publisher's Note: The statements, opinions and data contained in all publications are solely those of the individual author(s) and contributor(s) and not of MDPI and/or the editor(s). MDPI and/or the editor(s) disclaim responsibility for any injury to people or property resulting from any ideas, methods, instructions or products referred to in the content.